Journal of Molecular Liquids 368 (2022) 120789

Contents lists available at ScienceDirect

Journal of Molecular Liquids

journal homepage: www.elsevier.com/locate/molliq

# Thymol+l-menthol eutectic mixtures: Thermophysical properties and possible applications as decontaminants

Fernando Bergua [a,c], Miguel Castro [b,d], Carlos Lafuente [a,c], Manuela Artal [a,c,*]

[a] Departamento de Química Física, Facultad de Ciencias, Universidad de Zaragoza, Zaragoza, Spain
[b] Departamento de Ciencia y Tecnología de Materiales y Fluidos, Universidad de Zaragoza, Zaragoza, Spain
[c] Instituto Agroalimentario de Aragón - IA2 (Universidad de Zaragoza - CITA), Zaragoza, Spain
[d] Instituto de Nanociencia y Materiales de Aragón (INMA) Universidad de Zaragoza - CSIC, Zaragoza, Spain

ARTICLE INFO

*Article history:*
Received 8 September 2022
Revised 6 November 2022
Accepted 8 November 2022
Available online 12 November 2022

*Keywords:*
Thymol
L-menthol
Eutectic
Emerging contaminants
Thermophysical properties
Solubility and extraction

ABSTRACT

The substitution of conventional organic solvents for others with less environmental impact is one of the basic premises of green chemistry. To carry this out optimally, tools based on the similarity of thermophysical behaviour are being developed. Thus, the characterization of new solvents is a key step in any field of application. In this work, we studied the eutectic hydrophobic thymol + l-menthol system. The solid–liquid equilibrium of the system and several properties of three of its mixtures close to eutectic composition were measured and discussed. Calculations and correlations were performed to obtain properties of interest such as the internal pressure, critical temperature, and solubility parameter, among others. To predict the system behaviour under any operating conditions, the PC-SAFT equation of state was validated. Considering the problem of the presence of drugs as micro pollutants in the environment, the ability of this eutectic system to both dissolve drugs and remove them from contaminated water was also analysed. The results showed a strong thymol-l-menthol interaction, and a higher thymol ratio made the liquid more compact and structured but less polar and viscous. The difference in densities with respect to that of water and the moderate viscosity values indicated that this system can be an adequate solvent in liquid–liquid extraction processes. The solubilities of quercetin (Q), nitrofurantoin (NF) and tetracycline (TC) were enhanced in the eutectic mixtures; for Q, the solubility was 10000-fold higher than that in water. Finally, this system could be used to remove traces of Q and NF from the water, with an efficiency of up to 81 %.



## 1. Introduction

The goal of directive 1999/13/CE is the prevention of the effects associated with the emissions of volatile organic compounds (VOCs) on people and the environment. For that, limits and conditions of utilization are imposed. Industries can opt for the modification of their facilities or the substitution of VOCs by eco-friendly fluids. The second option is economically advantageous, but the chemical-physical properties of the neoteric solvent must be known and be similar to the one it replaces. Therefore, there must be tools containing a wide database of these properties to optimize the composition of the alternative fluids. The Program for Assisting the Replacement of Industrial Solvents (PARIS III) is the software developed by the United States Environmental Protection Agency (EPA)[1]. It uses the following concept: the solvent capacity of a fluid is a consequence of the values of its thermodynamic (activity coefficients, density, surface tension, and critical points) and transport (diffusivity and viscosity) properties. Based on them, each solvent is represented by coefficients, and the application provides a substitute with the closest values. Environmental and safety requirements are also considered. The search for new solvents is essential to the pharmaceutical industry. Several private companies and institutions, such as the ACS Green Chemistry Institute Pharmaceutical Roundtable, have updated solvent selection guides and online tools based on physicochemical affinity [2–4]. It should be noted that most of the active principles (APIs) are poorly soluble compounds in water [5]. Therefore, they present problems such as insufficient bioavailability, the delayed onset of action and erratic absorption [6]. Strategies such as the preparation of solid dispersions, formation of cocrystals and salts, emulsions or confinement in mesoporous silica [7] solve some of the problems. The formulations of the APIs in the liquid state could also avoid the inconve-

* Corresponding author at: Departamento de Química Física, Facultad de Ciencias, Universidad de Zaragoza, Zaragoza, Spain.
*E-mail address:* martal@unizar.es (M. Artal).

https://doi.org/10.1016/j.molliq.2022.120789
0167-7322/

niences associated with their possible polymorphism. They can be obtained by solubilisation using a drug vehicle. For this aim, conventional solvents are not adequate, and eutectic solvents (ESs) can be an alternative [5,8]. The ESs are mixtures whose experimental melting temperature ($T_m$) is lower than those of the pure compounds. They are known as deep eutectic solvents (DESs) if the difference between $T_m$ and the theoretical temperature assuming ideal behaviour $\left(T_m^{id}\right)$ is large, and they are called natural deep eutectic solvents (NADESs) if, in addition, the components are metabolites. The latter are especially interesting due to their low toxicity. Other properties can be mentioned, according to the green chemistry principles, such as their nonflammability and nonvolatility and their easy, cheap and lack of waste preparation; thus, DESs are being used in various applications [9–17]. Among other factors, the depression in $T_m$ is a consequence of the capability of the components to form hydrogen bonds. This network provides the liquid with high stability and facilitates the solubility of species with donor and acceptor groups. Recent studies [8,18–21] have reported the increased solubility and improved stability of drugs when they are dissolved in NADESs. For example, the solubility of itraconazole in a choline chloride:glycolic acid mixture is 6700 times greater than that in water, and the hydrolysis of aspirin is 8 times slower in choline chloride:1,2-propanediol. Similarly, there is a second way to obtain liquid pharmacological formulations. Considering that APIs usually contain chemical groups that can act as hydrogen bond donors or acceptors, they can form eutectic mixtures with an excipient or between them. These mixtures have therapeutic characteristics and are called THEDES [22]. Their main advantage is that the pharmacological properties of the APIs can be modified without structural changes. The literature reports an improvement in the bioavailability, permeability and therapeutic activity with respect to the solid form [20] of the drug. Bonain's liquid, first prepared in 1889, was the first therapeutic eutectic mixture [23]. It is composed of phenol, cocaine hydrochloride and menthol in an equivalent ratio and has anaesthetic effects. In 1992, the U.S. Food and Drug Administration approved the first commercial THEDES, the lidocaine:prilocaine equimolar mixture. It was formulated as an oil-in-water emulsion and exhibited higher efficacy than the compounds applied separately [24,25]. Later, mixtures with ibuprofen, aspirin or lidocaine, among others, were evaluated. The high API concentration in the mixture and the presence of permeation enhancers such as menthol or thymol favoured the diffusion of drugs [8]. The ever-increasing use of drugs and their high excretion percentage has made their presence in the environment a problem to be addressed by institutions [26]. In 2018, the water crisis was classified as one of the 5 main social risks (World Economic Forum's Global Risks Report 2018; https://reports.weforum.org/global-risks-2018). It is not only a problem of quantity but also of quality. Thus, a specific challenge of the European Green Deal says, 'Towards a zero-pollution ambition for a toxic free environment'. Its aim is focused on the removal of persistent chemicals, highlighting existing deficiencies in scientific knowledge. Eutectic mixtures with hydrophobic character have also been studied since 2015 as extraction solvents of persistent contaminants in aqueous medium [11,27–35]. Among them, we highlight those containing thymol (T) and menthol (M) from now called TM system, because both components are considered generally recognized as safe (GRAS) by the Environmental Protection Agency (EPA).

Thymol, a phenolic monoterpenoid, is the main component, close to 50 %, of the oil of thyme. It is a powerful fungicide and pesticide that has other uses in the cosmetic, agri-food and pharmaceutical industries. Menthol is a cyclic monoterpenoid alcohol that can be synthesized in the laboratory or extracted from plants in the menthe family. It has eight stereoisomers, with l-menthol being the only one with a natural origin. It also presents the best dermal properties, and has shown several therapeutic properties as an analgesic, antitussive, antiviral or anticancer, among others [36]. A synergistic effect of the TM eutectic system as an antimicrobial agent has been observed [37]. Despite the similarity of the structures of its components, this system exhibits a nonideal unexpected behaviour [38–41]. Therefore, the study of this THEDES is interesting both from a theoretical point of view and from its applicability. Several authors have analysed the solid–liquid phase transitions [38–41] and published density and viscosity data at atmospheric pressure [28,42–46]. No density under pressure or other properties were found in the literature; however, there is a greater number of publications about its extraction capacity. The extracts were usually chlorophenols, drugs, pesticides and organic acids, and the matrices were polluted water and biomass [28,43,44,46–52].

This article will focus on the thermophysical characterization of thymol:l-menthol mixtures to be implemented in industry as alternative solvents. Moreover, its ability to dissolve three APIs (quercetin, nitrofurantoin, and tetracycline) and its capacity to remove them from aqueous medium were evaluated. The manuscript has been organized as follows. In Section 2, the materials, devices, and methods used to obtain the experimental data are briefly described. Section 3 begins with the study of the solid–liquid phase change. The thermal events are described, and the experimental data are shown and thermodynamically modelled. Later, the results of the thermophysical characterization of three mixtures of TM systems are presented, correlated, and discussed. The measured properties are the density (from 0.1 to 65 MPa), speed of sound, refraction index, static permittivity, isobaric molar heat capacity, surface tension, and viscosity. Finally, solubility and extraction studies are reported. The solubility parameters of the solvents are calculated, and the feasibility of these DESs to dissolve poorly water-soluble drugs and remove them from aqueous medium is given. The article ends with Section 4, which includes a summary of the conclusions. The Supplementary Information (S. I.) contains the description of the correlations and models used in the characterization, all of the experimental values of the measured properties, and additional figures to the manuscript.

## 2. Materials and methods

### 2.1. Materials

The chemicals used as components of the eutectic mixtures were thymol (T) and l-menthol (M). We chose the l-menthol isomer because it is the main menthol form in nature. The active principles studied in the solubility and extraction experiments were quercetin (Q), nitrofurantoin (NF) and tetracycline (TC). All compounds were supplied by Sigma–Aldrich and were used without further treatment. Table 1 and Fig. 1 report the characteristics and structures of the compounds. The studied mixtures were thymol + l-menthol (TM) in the following three molar ratios: 1:2, 1:1, and 2:1. To prepare the mixtures, the pure compounds were weighed in adequate proportions using a PB210S Sartorius balance with an uncertainty of $1{\cdot}10^{-4}$ g. Subsequently, simultaneous stirring and heating were used to obtain a stable liquid phase over time. At this stage, the temperature was maintained close to 323 K to avoid the thermal degradation of the components. Table 2 reports the acronyms used in the manuscript for the TM mixtures, composition, molar mass ($M_w$), and melting temperature ($T_m$).

### 2.2. Calorimetric characterization

The solid–liquid equilibria (SLE) was obtained with a differential scanning calorimeter (TA Instruments DSC Q2000) with a RCS

**Table 1**
Relevant properties of pure compounds used in this work. Molar mass ($M_w$), melting temperature ($T_m$), melting enthalpy ($\Delta_m H$), dipole moment ($\mu$), and polarizability ($\alpha$).

| Chemical (acronym) | Purity[a] | $M_w$/ g·mol$^{-1}$ | $T_m$/ K | $\Delta_m H$/ kJ·mol$^{-1}$ | $\mu$/ D | $\alpha$/ Å$^3$ |
|---|---|---|---|---|---|---|
| Thymol (T) | >0.985 | 150.22 | 322.5 ± 0.5[b] 322.65 ± 1.1[d] | 17.3 ± 0.2[b] 19.2 ± 1.9[d] | 1.54[c] | |
| L-menthol (M) | >0.99 | 156.27 | 315.2 ± 0.5[e] 316.4 ± 0.9[d] | 13.1 ± 0.1[e] 12.9 ± 1.3[d] | 1.57[f] | |
| Quercetin (Q) | >0.95 | 302.24 | 589.6[g] | – | 2.8522[h] | 34.67[h] |
| Nitrofurantoin (NF) | >0.98 | 238.16 | 536.[g] | – | 4.91[i] | 19.85[i] |
| Tetracycline (TC) | >0.95 | 444.43 | 445.6[g] | – | 6.11[i] | 40.92[i] |

[a] As stated by the supplier (mass fraction).
[b] Ref. [34].
[c] Ref. [53].
[d] Ref. [54].
[e] Ref. [35].
[f] Ref. [55].
[g] Ref. [56].
[h] Ref. [57].
[i] Ref. [58].

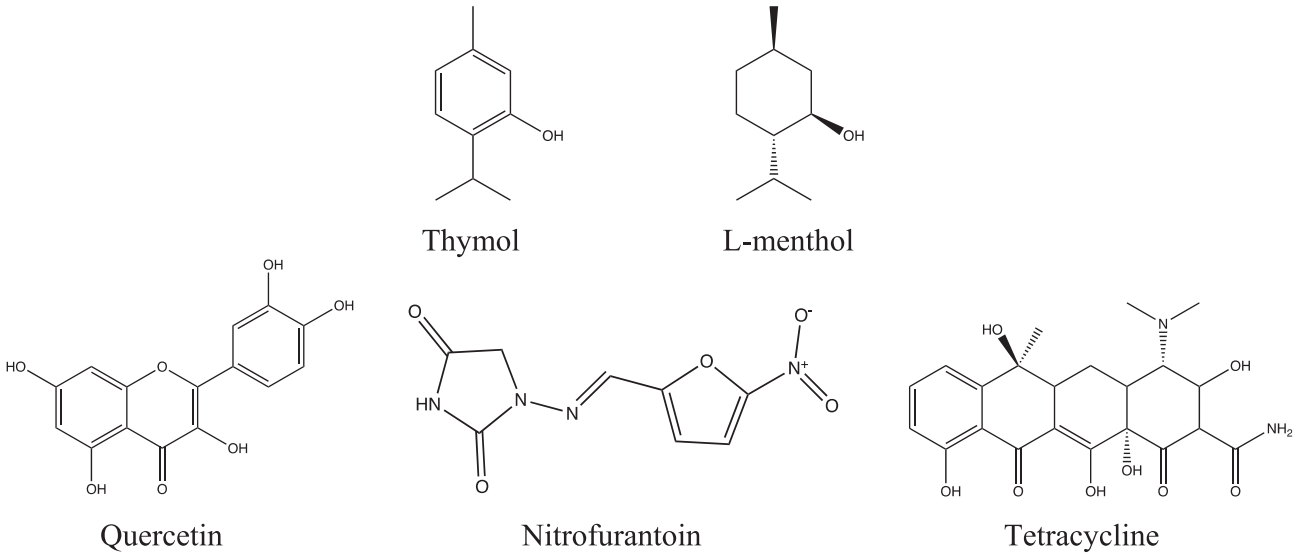


**Fig. 1.** Structure of the compounds used in this study.

**Table 2**
Characteristics of the studied thymol + l-menthol eutectic solvents ([TM]ESs).

| Acronym | Component 1 | Component 2 | Molar ratio | $M_w^a$/ g·mol$^{-1}$ | $T_m^b$/ K |
|---|---|---|---|---|---|
| TM12 | Thymol | L-menthol | 1:2 | 154.25 | 268.2 |
| TM11 | Thymol | L-menthol | 1:1 | 153.24 | – |
| TM21 | Thymol | L-menthol | 2:1 | 152.23 | 282.5 |

[a] $M_w = \sum_i M_{w,i} x_i$
[b] This work; $u(T_m) = 0.5$ K.

cooling system. A standard of Indium was used to carry out the temperature and heat flow calibrations by using its melting properties. The differences between the expected values of Indium and those obtained during the calibration showed that the uncertainties in $T_m$ and $\Delta_m H$ were 0.5 K and 1 kJ·mol$^{-1}$, respectively. For each mixture used to build the SLE diagram, a sample (5 to 15 mg) was weighed and introduced into an aluminum pan in liquid state. If the sample was solid at room temperature, once the pan was in the DSC a preheating step was performed up to a temperature higher than the melting point to ensure the crystallization of the mixture within the device. The samples were firstly cooled at 203–213 K at 3 K/min and later heated at the same scanning rate up to 10 above the phase change. The reported temperatures correspond to the maximum peak because of the asymmetric peak shapes and the presence of thermal anomalies which difficult the determination of the onset temperature.

On the other hand, sapphire was used in addition to Indium during the calibration to obtain the isobaric molar heat capacity values. Two different sapphire experiments were carried out, before and after each daily measurement session, to discard any temporal evolution of the heat capacity calibration factor.

### 2.3. Thermophysical properties

The thermophysical properties were measured with several thermostatised devices that are widely used in the literature. Therefore, no full description is given in this paper. Table 3 summarizes the standard uncertainty in the temperature ($u(T)$), the

calculated combined expanded uncertainties ($U_c(Y)$) for each property (0.95 level of confidence, $k$= 2), and the mean relative deviations ($MRD(Y)/\%$) in the checking of each piece of equipment.

### 2.4. Solubility and extraction

The thermodynamic solubilities ($W$) of Q, NF, and TC were measured in the three TM mixtures with the shake-flask method at a constant temperature of 298.15 K. The method is based on the addition of a solid solute until supersaturation is reached and subsequent analysis of the liquid phase. We used an ultrasonic bath with temperature control to facilitate solute–solvent mixing. For each result, five samples were prepared and mixed, and two aliquots of each sample were centrifuged and filtered (PES syringe filter, 0.22 μm). Then, every solubility result was the average value of ten analyses. The measurement had to correspond to the system in equilibrium, and thus, several analyses were performed at different mixing times (30 to 120 min). The value that remained constant was given as the thermodynamic solubility. The API concentration was measured by VIS-UVA spectrophotometry with VWR 6300 PC double-beam equipment ($u(\lambda)$=±0.2 nm). In the Supplementary Information (S.I.), Table S1 lists the equations of the calibration curves and their limits of detection and quantification.

The extraction efficiency, $EE$, was determined by liquid–liquid extraction taking advantage of the hydrophobic nature of this system. To do this, stock solutions of contaminated water were prepared and analysed to determine the API pre-extraction concentration, $C_i$. The values were $C_i(\mathrm{Q}) < 20\mu$ M, $C_i(\mathrm{NF}) < 50\mu$ M, and $C_i(\mathrm{TC}) < 60\mu$ M. Similar volumes of stock solution and eutectic solvent were mixed over 12 h in a double wall thermostatic flask at 298.15 K. After deposition and centrifugation, the postextraction concentration, $C_f$, was obtained. Each data point is the average of the analyses that reached thermodynamic solubility. The efficiency was calculated with the following equation: $EE = 100\left[\left(C_i - C_f\right)/C_i\right]$.

## 3. Results and discussion

Knowing the thermophysical behaviour of fluids under different pressure and temperature conditions is essential for their use in industry. If experimental values are not available, having prediction tools can be a good substitute, although they must first be validated. We report herein a comprehensive characterization of the thymol + l-menthol (TM) system. It includes the measurement and analysis of both the change in the solid–liquid phase of the system and the thermophysical properties of three mixtures of molar ratio compositions (1:2), (1:1), and (2:1). Additionally, several correlations and models were validated using the experimental values. A brief description of them is given in the S.I.

### 3.1. Solid–liquid equilibria

Table 1 lists the melting temperatures values and enthalpy of the pure thymol and l-menthol. The experimental values agreed with those of the literature considering the experimental uncertainties. For these mixtures, the thermograms had two main features. First, the enthalpy peaks were very small even at compositions far from the eutectic composition (Fig. 2). This could be due to the presence of micro heterogeneities formed by clusters of different sizes, which would result in the crystallization of only a small fraction of the sample [41,59]. On the other hand, no melting of the eutectic fraction ($T^E_{\mathrm{exp}}$) was detected in any of the experiments. Instead, glass transition temperatures ($T_g$) have been obtained (Fig. 3). For the equimolar mixture, there was no peak upon heating. The strong interactions between thymol and l-menthol provoke kinetic constraints on the formation of crystalline phases because the hydrogen bonds hinder the molecular rearrangement necessary for crystallization. The system transitions from a subcooled metastable state to a vitreous state [39]. As we move away from the eutectic composition, the kinetic restrictions decrease, and the molecules that are not part of the eutectic manage to rearrange themselves by crystallizing and subsequently melting. Alhadid et al. [39,40] only detected $T^E_{\mathrm{exp}}$, with a value of 241.45 K, if the sample was stored at 193 K for one month.

Table S2 lists the melting and glass temperatures determined in this work during the heating step. Mixtures of compositions within the range $0.16 < x_{\mathrm{Thy}} < 0.78$ were liquids at $T > 298.15$ K. This wide liquid window allows tuning the mixture with the most suitable thermophysical properties for each application. Our data of solid–liquid phase equilibria (SLE) and those from the literature are displayed in Fig. 4. The diagrams were similar, and the largest deviations were found in the interval $0.6 < x_{\mathrm{Thy}} < 0.8$, in which $T_m$ barely changed with $x_{\mathrm{Thy}}$. This fact is related to the presence of metastable solid-states [40]. The figure also includes $T_g$ points. Our average value of 213.76 K was only 0.6 % higher than that reported by Abranches [38].

A eutectic mixture can be named deep (DES) if its melting temperature is much lower than it would be if it were ideal. Therefore, it is convenient to estimate the ideal phase diagram of the system and to compare it with the experimental diagram. To do this, the

**Table 3**
Summary of the devices used in the thermophysical characterization.

| Property | Devices | $u(T)$/K | $U_c(Y)$[a] | $MRD(Y)$[b]/% |
|---|---|---|---|---|
| $\rho$ | Oscillating U-tube density meter, Anton Paar DSA 5000 | 0.005 | 0.05 kg·m$^{-3}$ | 0.004 |
| $p\rho T$ | Oscillating U-tube density meter, Anton Paar DMA HP 5000 | 0.005 | 0.1 kg·m$^{-3}$ | 0.015 |
| $u$ | Acoustic, time-of-flight method, Anton Paar DSA 5000 | 0.005 | 0.5 m·s$^{-1}$ | 0.026 |
| $C_{p,m}$ | Differential scanning calorimeter, TA Instruments DSC Q2000 | 0.5 | 1 % | 0.028 |
| $n_D$ | Standard Abbe refractometer, Abbemat-HP refractometer Dr. Kernchen | 0.01 | 2·10$^{-5}$ | 0.007 |
| $\varepsilon$ | Capacitance method, Agilent 4263BA LCR 2 MHz | 0.01 | 0.02 | 0.11 |
| $\gamma$ | Drop volume tensiometer, Lauda TVT-2 | 0.01 | 1 % | 0.21 |
| $v$ | Capillary viscosimeter Ubbelohde, Schoot-Geräte AVS-440 | 0.01 | 1 % | 0.28 |

[a] k = 2 (0.95 level of confidence).
[b] $MRD(Y) = \frac{100}{n}\sum_{i=1}^{n}\left|\frac{Y_{i,\mathrm{lit}} - Y_{i,\mathrm{exp}}}{Y_{i,\mathrm{exp}}}\right|$,

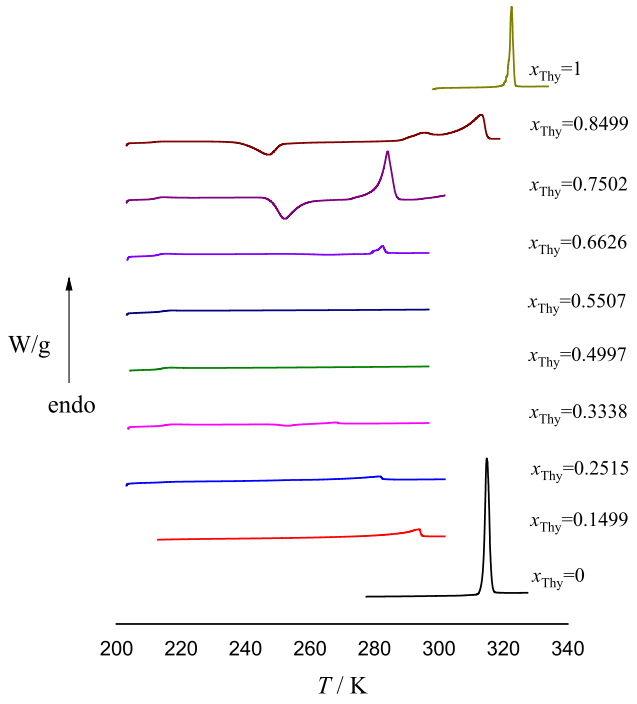


**Fig. 2.** Thermograms of [TM]ESs.

thermodynamic equation that provides the solubility of a solid in the liquid phase is used. Neglecting the term corresponding to the variation in the heat capacity, the expression is:

$$\ln\left(x_i\gamma_i^l\right) = \frac{\Delta_m H_i}{R}\left(\frac{1}{T_{m,i}} - \frac{1}{T_m}\right) \quad (1)$$

where $\gamma_i^l$ is the activity coefficient in the liquid phase of component $i$ at composition $x_i$;$T_{m,i}$ and $\Delta_m H_i$ are the melting temperature and melting enthalpy of component $i$; and $T_m$ is the melting temperature of the mixture. For $\gamma_i^l$ = 1, the calculated solubilities are those assuming ideal behaviour. Although we were unable to measure $T^E_{exp}$, Fig. 4 shows a clear negative deviation from ideality, with a $(T^E_{exp} - T^E_{id})$ of approximately 40 K. Then, the TM system could be named a DES.

The measured $T_m$ values were correlated with the nonrandom two-liquid model (NRTL) (S.I.)[60]. The model parameters were $A_{12} = -3363.16$ J·mol$^{-1}$ and $A_{21} = -5820.78$ J·mol$^{-1}$, and the estimated eutectic points were $x^E_{Thy,NRTL}$ =0.4651 and $T^E_{Thy,NRTL} = 232.65K$. The activity coefficients ($\gamma_i$) were also calculated and are listed in Table S2. From them, a deviation from ideality more pronounced at higher $x_{Thy}$ was observed. These results can be explained by the resonant effects of thymol when delocalizing the free pair of electrons from oxygen. For Eq. (1), $\gamma_i^l$ can be calculated with a thermodynamic model as the ratio between the fugacity coefficients of component $i$ in the mixture and in the pure state. Herein, we used the PC-SAFT equation of state (EoS) (S.I.)[61,62]. The parameters necessary for the calculation are given in Table S3, and the estimated curve is included in Fig. 4. The mean relative deviation calculated between the experimental and predicted melting temperatures for the three characterized mixtures was lower than 1 % (Table S4), and the average value for the SLE was $MRD(T_m)$ = 1.5 %.

### 3.2. Thermophysical study of TM mixtures

The studied properties were density ($\rho$), speed of sound ($u$), refraction index ($n_D$), static permittivity ($\varepsilon$), isobaric molar heat capacity ($C_{p,m}$), surface tension ($\gamma$), and dynamic viscosity ($\eta$). They were determined at $p = 0.1$ MPa and at temperatures ranging from 278.15 to 338.15 K. The experimental data at each temperature, composition and at 0.1 MPa are collected in Table S5. The density was also measured up to 65 MPa in the $T$ range of 283.15–338.15 K, and the $p\rho T$ values are listed in Table S6. Moreover, the experimental and calculated values at 298.15 K for different properties are collected in Table 4 to ease the follow-up of the discussion.

Standard uncertainties are: $u(T)$=0.005 K for density and speed of sound and 0.01 K for the rest of properties; $u(p)$=0.5 kPa. The combined expanded uncertainties (0.95 level of confidence, $k$=2) are$U_c(\rho)$ = 0.05 kg·m$^{-3}$; $U_c(u)$=0.5 m·s$^{-1}$; $U_c(C_{p,m})$=1%; $U_c(n_D)$=2·10$^{-5}$; $U_c(\varepsilon) = 1$ %; $U_c(\gamma)$=1%; $U_c(\eta)$=1%; $U_c(\alpha_p)$=0.04 kK$^{-1}$; $U_c(\kappa_T)$=0.22 TPa$^{-1}$; $U_c(\kappa_s)$=0.22 TPa$^{-1}$; $U_c(L_f)$=0.005 Å; $U_c(R_m)$=0.004 cm$^3$·mol$^{-1}$; $U_c(f_m)$=0.03 cm$^3$·mol$^{-1}$; $U_c(\Delta S_S)$=0.001 mN·m$^{-1}$·K$^{-1}$; $U_c(\Delta H_S)$=0.06 mN·m$^{-1}$.

The densities at 0.1 MPa ranged (Fig. S1) from 890.67 kg·m$^{-3}$ for TM12 at 338.15 K to 953.12 kg·m$^{-3}$ for TM21 at 288.15 K. At the same compositions and temperatures and 65 MPa, they were 928.82 and 985.50 kg·m$^{-3}$, respectively. On average, $\rho$ was 6.5 % lower than that of water at similar $p$ and $T$, which can ensure an adequate phase separation in the liquid–liquid processes [28]. The density increased with increasing thymol molar ratio ($x_{Thy}$), which is logical since thymol is a flatter molecule than l-menthol due to the presence of the aromatic ring. Several authors [28,42–45] have published densities of the TM system at atmospheric pressure. The values were in agreement with ours, with an average mean relative deviation of 0.12 %. The graphic comparison is shown in Fig. S2a. No $p\rho T$ data were found in the literature. As usual, $\rho$ decreased with increasing temperature and decreasing pressure. Thermal agitation weakens the interactions in the mixture, while decreasing the free volume increases the number of

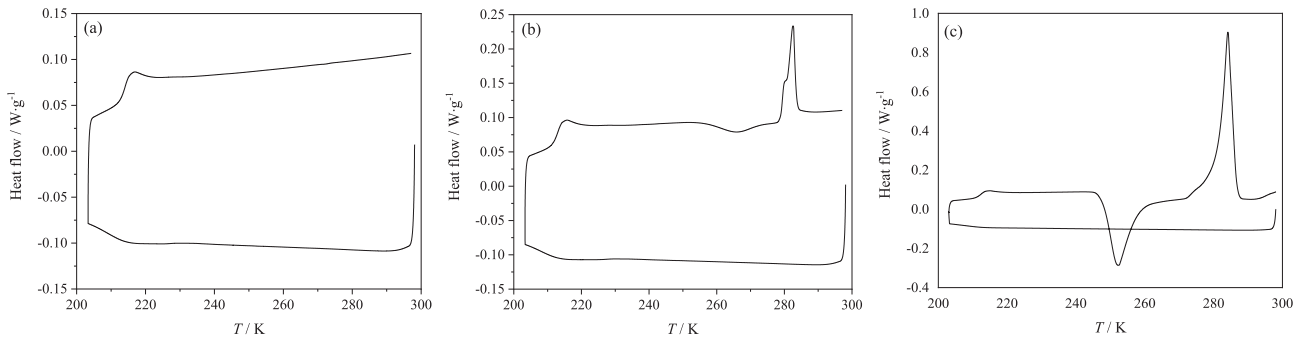


**Fig. 3.** Detailed thermograms of [TM]ESs at several compositions: (a) $\chi_{Thy}$ = 0.4997; (b) $\chi_{Thy}$= 0.6626; and (c) $\chi_{Thy}$= 0.7502.

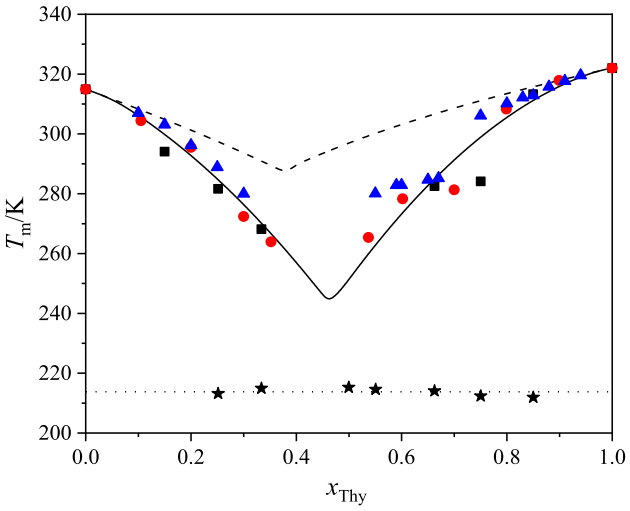


**Fig. 4.** Solid–liquid equilibria of the thymol + l-menthol system. (■), This work; (●), Ref. [38]; (▲), Ref. [40]; (⋆), Glass transition temperature, this work. (– –), ideal; (——), NRTL model.

**Table 4**
Summary of the thermophysical properties at $T = 298.15$ K and $p = 0.1$ MPa of the [TM]ESs.

| Property | TM12 | TM11 | TM21 |
|---|---|---|---|
| $\rho$/kg · m$^{-3}$ | 921.09 | 932.93 | 945.59 |
| $u/m$ · s$^{-1}$ | 1386.99 | 1396.13 | 1406.03 |
| $n_D$ | 1.47903 | 1.48953 | 1.49914 |
| $\varepsilon$ | 5.857 | 5.659 | 5.329 |
| $C_{p,m}$/J · mol$^{-1}$ · K$^{-1}$ | 317 | 319 | 319 |
| $\gamma$/mN · m$^{-1}$ | 29.21 | 29.70 | 30.32 |
| $\eta$/mPa · s | 41.048 | 35.275 | 26.102 |
| $\alpha_p$/kK$^{-1}$ | 0.777 | 0.767 | 0.779 |
| $\kappa_T$/TPa$^{-1}$ | 651.05 | 635.85 | 612.86 |
| $\pi_T$/MPa | 355.73 | 359.55 | 378.87 |
| $\kappa_S$/TPa$^{-1}$ | 564.35 | 549.92 | 534.94 |
| $L_f$/Å | 0.470 | 0.464 | 0.457 |
| $R_m$/cm$^3$ · mol$^{-1}$ | 47.491 | 47.450 | 47.284 |
| $f_m$/cm$^3$ · mol$^{-1}$ | 119.97 | 116.81 | 113.72 |
| $g\mu^2$/D$^2$ | 4.07 | 3.71 | 3.26 |
| $\Delta S_S$/mN · m$^{-1}$ · K$^{-1}$ | 0.080 | 0.079 | 0.081 |
| $\Delta H_S$/mN · m$^{-1}$ | 52.98 | 53.40 | 54.59 |
| $E_{a,\eta}$/kJ · mol$^{-1}$ | 61.0 | 58.8 | 53.8 |

molecules per unit volume. At 0.1 MPa, this behaviour is shown in Fig. S1a. The behaviour under pressure is displayed in Fig. 5a for the TM11 mixture and Fig. S3 for the rest of the mixtures. The equations of the relationships are summarized in S.I. Table 5 reports the parameters of the $\rho T$ relationship at 0.1 MPa, and Table 6 lists those of $p\rho T$.

We quantified the effect of the temperature and pressure on the density with the calculation of the isobaric thermal expansibility ($\alpha_p$) and the isothermal compressibility ($\kappa_T$):

$$\alpha_p = -\frac{1}{\rho}\left(\frac{\partial \rho}{\partial T}\right)_p \tag{2}$$

$$\kappa_T = \frac{1}{\rho}\left(\frac{\partial \rho}{\partial p}\right)_T \tag{3}$$

For each $p$ and $T$, $\alpha_p$ hardly changes as the molar ratio of thymol increases. On the other hand, the expansion capacity of the mixtures increased with increasing temperature or decreasing pressure according to the weakening of the forces between the components (Fig. 5b and S4). The effect of $T$ on $\alpha_p$ was more pronounced at lower pressure, and the effect of $p$ on $\alpha_p$ was more pronounced at higher temperature. For example, for TM12 at 0.1 MPa, $\alpha_p$ ranged from 0.730 k·K$^{-1}$ at 283.15 K to 0.911 k·K$^{-1}$ at 338.15 K. At 65 MPa, the values were 0.620 and 0.704 k·K$^{-1}$, respectively.

The $\kappa_T$ calculated values showed that the more compact the mixture was, the higher the thymol ratio. Thus, TM21 was, on average, 4 % less compressible under isothermal conditions than TM12. This property increased when the temperature increased, especially at lower pressures, and with higher pressure decreased mostly at higher temperatures (Fig. 5c and S5). The internal pressure ($\pi_T$) is defined as the change in internal energy of a system when the volume changes at constant temperature. The $\pi_T$ sign indicates the type of intermolecular forces prevailing in the system. The more positive the internal pressure is, the greater the attractive forces. It can be calculated from $\alpha_p$ and $\kappa_T$ data:

$$\pi_T = T\left(\frac{\alpha_p}{\kappa_T}\right) - p \tag{4}$$

For the studied mixtures, Table 4 collects the values at 298.15 K, which increased with increasing thymol ratio. This result highlights the importance of the $\pi-$ interactions. To validate the PC-SAFT EoS for the volumetric behaviour, we calculated the densities in the $p$ and $T$ working ranges of this work and compared them with the experimental densities. The model slightly overestimated the $p\rho T$ data with an average deviation of 1.21 % for the TM system. No trends were observed with composition and temperature, but the higher the pressure was, the greater the deviation. The maxima deviations were 0.83 and 2.00 % at 0.1 and 65 MPa, respectively. Table S4 lists the deviation values, and Fig. S6a shows the graphic comparison for the TM11 mixture; the remaining compositions were similar.

The compactness of a fluid can also be evaluated in terms of the free intermolecular length ($L_f$) and the free volume ($f_m$). These properties can be calculated from $\rho, u$ and $n_D$ experimental data with the following expressions:

$$L_f = K\sqrt{\kappa_s} = \frac{K}{\sqrt{\rho u^2}} \tag{5}$$

$$f_m = V_m - R_m = V_m\left(1 - \frac{(n_D^2 - 1)}{(n_D^2 + 2)}\right) \tag{6}$$

where $K = f(T)$ is Jacobson's constant [63]; $\kappa_s$ is the isentropic compressibility; and $V_m$ and $R_m$ are the molar volume and refraction, respectively. The more compact the fluid is, the higher the speed of sound and the refraction index and, consequently, the lower the values of $\kappa_s$, $L_f$, $R_m$, and $f_m$. In fact, the effect of the composition and temperature on these properties (Table 4, Fig. S1b, S1c, S7) was similar to that obtained for the volumetric properties. The linear fit parameters of the $u - T$ and $n_D - T$ equations are found in Table 5. For $L_f$ and $f_m$, the calculated values ranged from 0.422 to 0.567 Å and 112.48 to 125.56 cm$^3$·mol$^{-1}$, respectively. Considering $V_m$, the percentage of free volume ($f_m/V_m$) of each mixture was within 71.3–72.5 % for TM12, 70.8–72.0 % for TM11, and 70.4–71.5 % for TM21. It is known that the PC-SAFT EoS does not adequately predict the values of the speed of sound, and the way to improve this prediction entails the modification of the universal constants of the model. For that, a deeper study of the question must be carried out in the future. In this work, the calculated $u$ values were less than those measured with an average $MRD(u) =$ 15 %. The deviations increased with decreasing $T$ and $x_{Thy}$, and the maximum deviation was 18 % (Table S4).

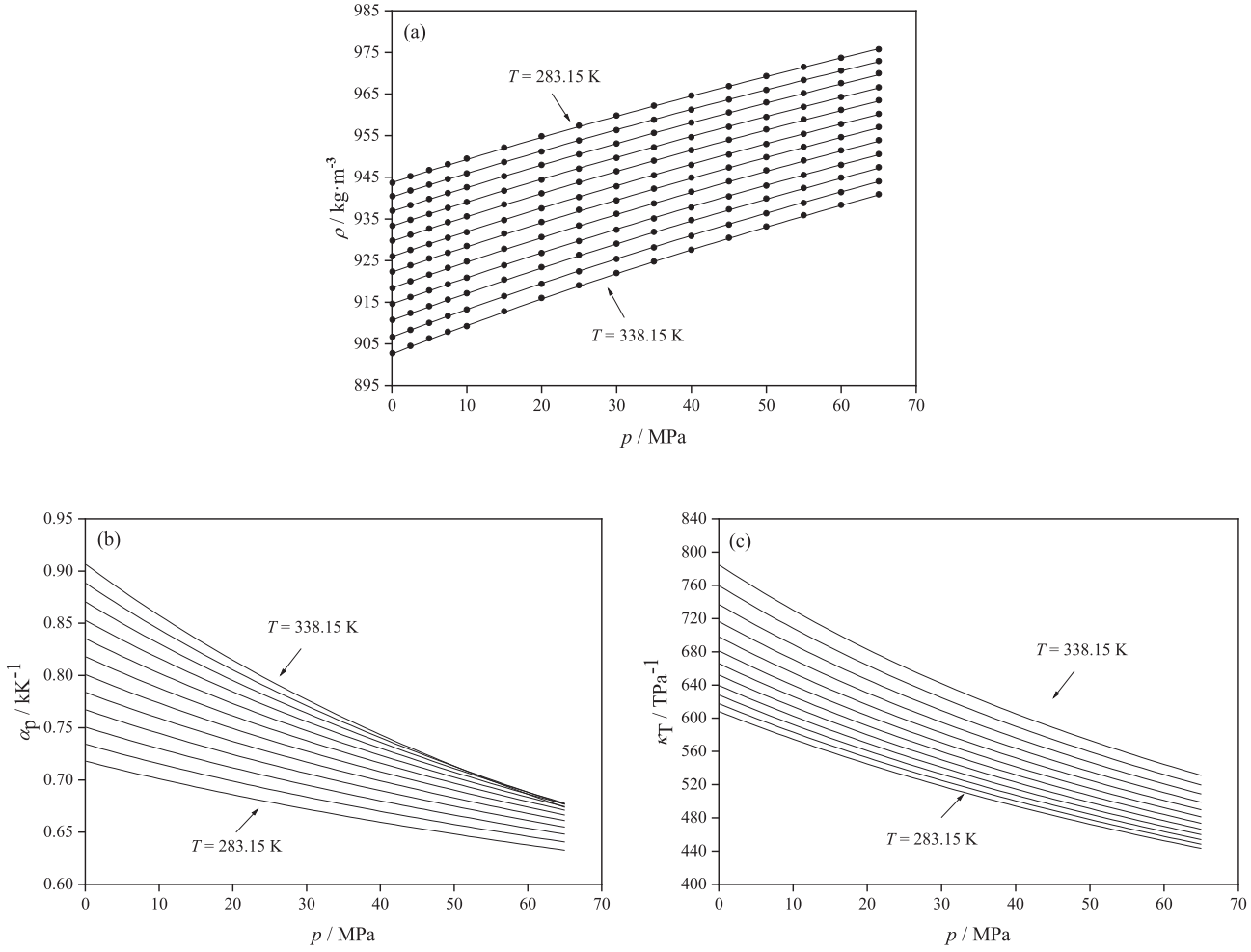


**Fig. 5.** Volumetric properties of the TM11 mixture as a function of temperature, $T$, and pressure, $p$. (a) Density, $\rho$; (b) isobaric expansibility, $\alpha_p$; and (c) isothermal compressibility, $\kappa_T$. (●) experimental data, (—) values calculated with the Tait equation.

**Table 5**
Fit parameters ($A_Y, B_Y, C_Y$) and the regression coefficients, $R^2$, for the thermophysical properties of the [TM]ESs.

| Property | [TM]ESs | $A_Y$ | $B_Y$ | $C_Y$ | $R^2$ |
|---|---|---|---|---|---|
| $\rho^a$/kg · m$^{-3}$ | TM12 | 1144.76 | − 0.7506 | | >0.99 |
| | TM11 | 1157.01 | − 0.7519 | | >0.99 |
| | TM21 | 1174.54 | − 0.7679 | | >0.99 |
| $u^a$/m · s$^{-1}$ | TM12 | 2422.21 | − 3.4726 | | >0.99 |
| | TM11 | 2421.11 | − 3.4379 | | >0.99 |
| | TM21 | 2416.34 | − 3.3882 | | >0.99 |
| $n_D^a$ | TM12 | 1.60422 | $-4.20 \cdot 10^{-4}$ | | >0.99 |
| | TM11 | 1.61647 | $-4.26 \cdot 10^{-4}$ | | >0.99 |
| | TM21 | 1.62886 | $-4.35 \cdot 10^{-4}$ | | 1 |
| $\varepsilon^a$ | TM12 | 10.99 | − 0.017 | | >0.99 |
| | TM11 | 9.76 | − 0.014 | | >0.99 |
| | TM21 | 9.01 | − 0.012 | | >0.99 |
| $C_{p,m}^a$/J · mol$^{-1}$ · K$^{-1}$ | TM12 | 25.718 | 0.97851 | | 1 |
| | TM11 | 79.544 | 0.80489 | | 1 |
| | TM21 | 68.660 | 0.83800 | | 1 |
| $\gamma^a$/mN · m$^{-1}$ | TM12 | 53.02 | − 0.0797 | | >0.99 |
| | TM11 | 53.48 | − 0.0795 | | >0.99 |
| | TM21 | 54.60 | − 0.0814 | | >0.99 |
| $\eta^b$/mPa · s | TM12 | 0.02921 | 636.50 | 210.33 | 1 |
| | TM11 | 0.03253 | 615.21 | 210.22 | 1 |
| | TM21 | 0.05995 | 507.10 | 214.70 | 1 |

[a] $Y = A_Y + B_Y T$
[b] $Y = A_Y \exp(\frac{B_Y}{T - C_Y})$

**Table 6**
Parameters of the Tait equation and the corresponding standard deviations, $MRD(\rho)^a$, of the [TM]ESs.

| | TM12 | TM11 | TM21 |
|---|---|---|---|
| $A_0$/kg · m$^{-3}$ | 1028.23 | 1033.09 | 1084.32 |
| $A_1$/kg · m$^{-3}$ · K$^{-1}$ | −3.93·10$^{-3}$ | 4.66 · 10$^{-2}$ | −1.89Å · 10$^{-2}$ |
| $A_2$/kg · m$^{-3}$ · K$^{-2}$ | -1.19Å · 10$^{-3}$ | −1.28Å · 10$^{-3}$ | −9.19Å · 10$^{-4}$ |
| $C$ | 0.0992 | 0.0956 | 0.0986 |
| $B_0$/MPa | 238.57 | 41.2 | 307.49 |
| $B_1$/MPa · K$^{-1}$ | 0.05965 | 1.29315 | − 0.26236 |
| $B_2$/MPa · K$^{-2}$ | -1.17Å · 10$^{-3}$ | −3.11Å · 10$^{-3}$ | −7.70Å · 10$^{-4}$ |
| $MRD(\rho)$/% | 0.014 | 0.011 | 0.008 |

The static permittivity allows the polarity of nonionic fluids to be analysed. For that,$\varepsilon$, $\rho$ and $n_D$ data under the same conditions are necessary, and the Fröhlich equation [64] is used:

$$g\mu^2 = \frac{9kT\varepsilon_0 V_m}{N_A}\frac{(\varepsilon - n_D^2)(2\varepsilon + n_D^2)}{\varepsilon(n_D^2+2)^2} \quad (7)$$

where $\varepsilon_0$ is the vacuum static permittivity and $\mu$ is the dipole moment of the mixture estimated from those of the pure components ($\mu^2 = x_1\mu_1^2 + x_2\mu_2^2$). The $g$ factor is the Kirkwood–Fröhlich correlation parameter and is related to the orientation of the neighbouring dipoles. Therefore, $g > 1$ for fluids with parallel preferential disposal and $<1g$ for those with antiparallel dipoles. Taking the $\mu_i$ data found in the literature (Table 1), we calculated the $g$ parameter for each TM mixture. The values ranged from 1.33 to 1.69, were higher at lower $x_{Thy}$, and barely changed with $T$. This result indicated a parallel preferred orientation between dipoles for all mixtures. The polarisation is also evaluated with the orientational dipolar parameter ($g\mu^2$). Bouteloup et al. [65] published $g\mu^2$ data for pure thymol and l-menthol. The calculated values for the TM mixtures (Table 4) were much higher than those, which indicates that this parameter is not additive. Taking into account Eq. (7), similar trends of $\varepsilon$ and $g\mu^2$ with $T$ must be expected. The $\varepsilon - T$ fit coefficients are listed in Table 5. Nevertheless, the opposite is observed, as shown in Fig. S1d and S8. This fact was already observed for other liquids, such as eutectic mixtures containing thymol or l-menthol and carboxylic acids [34,35]. This is related to the increase in the effective dipole of the system caused by thermal agitation favouring the linear form of the aggregates over the cyclic form.

To characterize variable temperature processes, it is necessary to know the thermal behaviour of solvents. This includes knowing both its phase diagram and its ability to store heat. The measured values of the isobaric molar heat capacity were within 298 and 357 J·mol$^{-1}$·K$^{-1}$. They were similar for all TM mixtures, which can be explained by their similarity of nature and molar mass. The $C_{p,m}$ value is related to the accessible vibration modes of the molecules, and its number increases with $T$. Therefore, unlike the rest of the thermophysical properties studied here, the slope of the $C_{p,m} - T$ equation was positive (Table 5, Fig. S1e). Taherzadeh et al. [66] have proposed a correlation to estimate the $C_{p,m}$ of deep eutectic solvents from the molar mass and critical properties (S.I.). The average deviation between our experimental and correlated values was 7.3 %, increasing with $x_{Thy}$, and it was slightly higher than the predictive capacity of the model, 5.3 %, published by the authors. Moreover, we used the PC-SAFT EoS to calculate $C_{p,m}$. Similar to $u$, the model underestimated the values, although to a lesser extent. The average and maximum deviations were 5.64 and 8.73 %, respectively. Unlike for $u$, the trends were opposite. $MRD(C_{p,m})$ increased with increasing $T$ and $x_{Thy}$, as shown in Fig. S6b.

The surface tension of a liquid is a measure of the cohesive forces in the bulk. The more structured the system is, the higher the $\gamma$ value. It is an essential property in processes including solvent atomization. The experimental values for the TM system varied from 27.35 to 31.18 mN·m$^{-1}$. In agreement with the above results, TM21 presented the highest values. The rise of energy favours chaos in the fluids, and thus, the slope of the equation is negative (Table 5), as shown in Fig. 6a. The obtained values of the thermodynamic properties of the surface per unit surface area at 298.15 K are found in Table 4. The entropy ($\Delta S_S = -(\partial\gamma/\partial T)_p$)

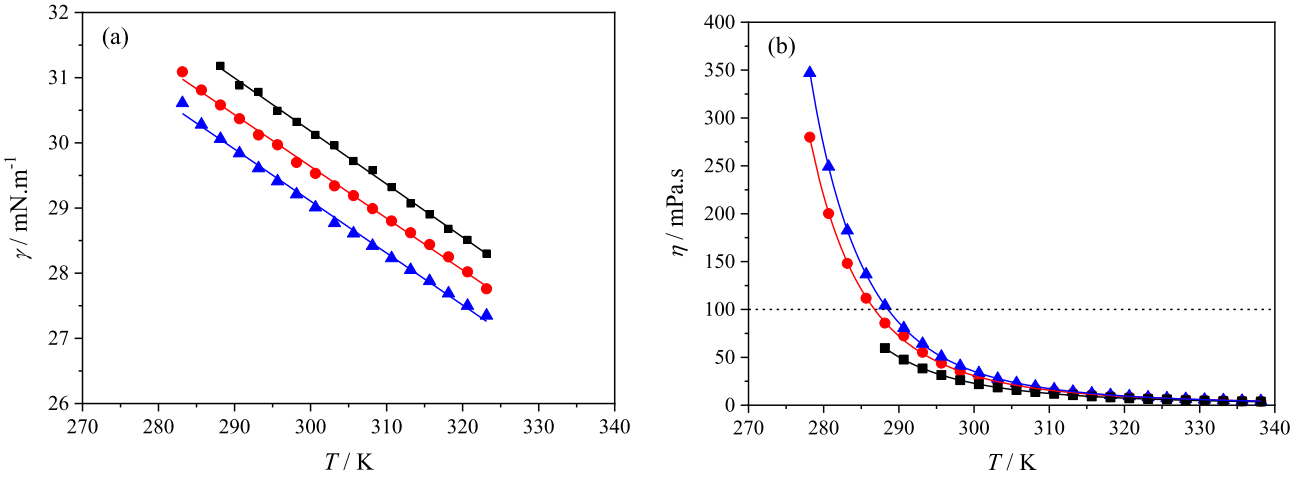


**Fig. 6.** Thermophysical properties of [TM]ESs as a function of temperature, $T$, and at different molar ratios: (▲), (1:2); (●), (1:1); and (■), (2:1). (a) Surface tension, $\gamma$; (b) dynamic viscosity, $\eta$. Points, experimental values; lines, correlated data.

was similar for the three mixtures, and the enthalpy ($\Delta H_S = \gamma - T(\partial\gamma/\partial T)_p$) increased with the thymol ratio. The authors have proposed equations that relate the surface tension to the critical temperature ($T_c$) of fluids. This is interesting because knowing the $T_c$ value is imperative for the application of thermodynamic models, but its measurement is sometimes not possible. In this work, we applied the Guggenheim and Eötvos correlations (S.I.) [67,68] as well as the PC-SAFT EoS. The calculated data are reported in Table S7. Assuming that the latter is an adequate model for the TM system, the average deviations for the two correlations were less than 3 %. Fig. S9 displays the predicted critical locus, $T_c - x_{\text{Thy}}$ and $p_c - x_{\text{Thy}}$ curves, for the system.

Finally, we analysed the fluidity of the TM hydrophobic mixtures. They presented moderately high values at low temperatures, reaching 347 mPa·s for TM12. The literature suggests that 100 mPa·s can be the maximum viscosity value to ensure a proper mass transfer process [28]. According to that, the operating temperature with the TM mixtures must be higher than 288 K to achieve their best functionality. In Fig. S2, a comparison with the literature [28,42,45] is shown. The values were different between the authors, and our results were in agreement with those of Martins et al. [42] with a deviation of 6.4 %. The change in temperature has an important effect on this property, as seen in picture $\eta - T$ (Fig. 6b), which fits an exponential mathematic function whose coefficients are listed in Table 5. The pre-exponential factor ($A_Y$) is the viscosity of the fluid at $T = \infty$, that is, without molecular interactions, and the rest of coefficients ($B_Y, C_Y$) allow us to calculate the energy of the viscous flow ($E_{a,\eta}$); that is, the barrier that must be overcome for a molecule to move around others:

$$E_{a,\eta} = R\partial(\ln\eta)/\partial(1/T) \tag{8}$$

Fig. S10 shows the polynomial decay of $E_{a,\eta}$ with $T$. The $E_{a,\eta}$ values were higher for TM12, and thus, we can say that this mixture has greater interactions between layers. We used the Pelofsky and Murkerjee equations [69] to correlate the viscosity and surface tension properties. The expressions and coefficients are collected in the S.I. and Table S8. The linear regression coefficients indicated that the Murkerjee equation was a better representation for our system.

### 3.3. Solubility and extraction efficiency

One of the most important parameters to characterize the solvent power of a fluid is the parameter of solubility ($\delta$). It was defined by Hildebrand [70] as the root of the cohesive energy density (CED):

$$\delta = \sqrt{\frac{\Delta E_{vap}}{V_m}} \tag{9}$$

where $\Delta E_{vap}$ and $V_m$ are the enthalpy of vapourisation and the molar volume of the solvent, respectively. The $\delta$ values could be obtained from experimental measures of $\Delta E_{vap}$, but sometimes it is not possible due to the thermal degradation of substances. Thus, other experimental properties related to the structuring of the liquid can be used, such as density and surface tension. If $p\rho T$ data are available, as in this work, the CED can be approximated to the internal pressure. From $\gamma$ and $\rho$ data under the same conditions, several equations have been proposed to obtain $\delta$. We have used that proposed by Pereira and Vebber [71] based on Stefan's rule. The equations are as follows:

$$\delta = \sqrt{\pi_T} \tag{10}$$

$$\delta = 8.276\sqrt{\frac{\gamma}{V_m^{1/3}}} \tag{11}$$

The units of $\gamma$ and $V_m$ are mN·m $^{-1}$ and cm$^3$·mol $^{-1}$, respectively. Additionally, the PC-SAFT EoS predicted the Hildebrand parameter.

Later, Hansen [72] separated the cohesive energy into three contributions due to the different attractive interactions: dispersive ($\delta_d$), polar ($\delta_p$), and hydrogen bonds ($\delta_H$). Thus, the total Hansen solubility parameter (HSP) denoted $\delta_T$ ($= \delta$) is calculated as:

$$\delta_T^2 = \delta_d^2 + \delta_p^2 + \delta_H^2 \tag{12}$$

The dispersive interactions are proportional to the square of the polarizability ($\alpha$) and cause very small fields that disperse the light through the materials. Then, $\delta_d$ is related to the refraction index [73]. The polar contribution includes both the dipole–dipole attractions, proportional to the fourth power of the dipole moment ($\mu$), and the dipole–dipole induction, proportional to $\alpha\mu^2$. Hansen and Beerbower [74] proposed a simplified equation to estimate $\delta_p$. The last contribution is estimated from the energy of vapourisation of the OH − O hydrogen bond from infrared spectroscopy [75]. The equations for the three contributions (MPa$^{1/2}$) are:

$$\delta_d = 2.24 + 53\frac{n_D^2 - 1}{n_D^2 + 2} - 58\left(\frac{n_D^2 - 1}{n_D^2 + 2}\right)^2 + 22\left(\frac{n_D^2 - 1}{n_D^2 + 2}\right)^3 \tag{13}$$

$$\delta_p = 37.4\frac{\mu}{\sqrt{V_m}} \tag{14}$$

$$\delta_H = \sqrt{\frac{20920N}{V_m}} \tag{15}$$

where $N$ is the number of hydroxyl groups in the solvent and the units of $\mu$ and $V_m$ are D and cm$^3$·mol $^{-1}$.

Literature [76] reports HSP values of thymol and l-menthol estimated by group contribution methods. Then, we also calculated those for the mixtures as:

$$\delta_T = (\delta_{HSP})_{mix} = \sum_i \varphi_i(\delta_{HSP})_i \tag{16}$$

where $\varphi_i$ is the volume fraction of component $i$ in the mixture and $(\delta_{HSP})_i$ is each parameter.

All of the calculated values are listed in Table 7. The similarity of the values obtained from different thermophysical properties indicates the goodness of the results. The highest average deviation, 10 %, was found to compare with $\delta_T$ estimated from the group contribution method. The Hildebrand parameter was slightly higher than the total HSP (Eq. (12)), and the effect of the composition was only noticeable in the polar contribution.

**Table 7**
Solubility parameters of the [TM]ESs.

| | $\delta$/MPa$^{-1}$ | | | $\delta_d$/MPa$^{-1}$ | $\delta_p$/MPa$^{-1}$ | $\delta_H$/MPa$^{-1}$ | $\delta_T$/MPa$^{-1}$ | $\delta_T$/MPa$^{-1}$ |
|---|---|---|---|---|---|---|---|---|
| | (ec.10) | (ec.11) | (PC-SAFT) | (ec.13) | (ec.14) | (ec.15) | (ec.12) | (ec.16) |
| TM12 | 18.86 | 19.05 | 19.95 | 13.11 | 4.51 | 11.18 | 17.81 | 20.83 |
| TM11 | 18.96 | 19.27 | 20.34 | 13.24 | 5.30 | 11.29 | 18.19 | 21.02 |
| TM21 | 19.46 | 19.54 | 20.56 | 13.36 | 6.11 | 11.40 | 18.60 | 21.18 |

Next, the experimental results of the thermodynamic solubility ($W_i = g_i/g_{solvent}$) of quercetin (Q), nitrofurantoin (NF), and tetracycline (TC) in the characterized eutectic mixtures are presented. The first two APIs are insoluble in water, and the third is very slightly soluble (Table 8). In [TM]ESs, the solubility was increased in all cases, and it was especially pronounced for Q (Fig. 7a). Note that the trend of $W_Q$ with $x_{Thy}$ was opposite to those found for $W_{NF}$ and $W_{TC}$. The studied drugs present different characteristics. From Table 1 and Fig. 1, it can be seen that Q has the smallest dipole moment of the three drugs but a high polarizability, and TC has the highest value of both properties. In relation to the formation of hydrogen bonds, Q and TC present a large number of donor and acceptor sites. On the other hand, NF exhibits the weakest interactions. The dissolution process can be summarized in three stages: relaxation of solute–solute and solvent–solvent interactions, relocation of the solvent around the solute, and establishment of new solute–solvent interactions. That is, thermodynamic solubility depends on entropic and enthalpic aspects. The former is related to the free volume of the solvent, which we calculated in the above section from the thermodynamic properties. The second is a consequence of the balance between cohesive and adhesive forces in the solute–solvent system. Fig. 8 illustrates both effects. Due to the number of hydroxyl groups and the flat structure, the Q solubility was favoured in the least compact solvent. On the other hand, the enthalpic factor prevailed for NF and TC.

**Table 8**
Solubility ($W_i = g_i/g_{solvent}$) at $T$ = 298.15 K, of quercetin (Q), nitrofurantoin (NF), and tetracycline (TC), in water and in the [TM]ESs.

| Solvent | $10^3 W_Q$ | $10^3 W_{NF}$ | $10^3 W_{TC}$ |
|---|---|---|---|
| Water | $(2.3 \pm 0.2)\cdot10^{-4}$ [a] | 0.081 ± 0.4[a] | 0.76 ± 0.6[a] |
| TM12 | 2.50 ± 0.17 | 0.16 ± 0.01 | 21.8 ± 1.6 |
| TM11 | 1.17 ± 0.06 | 0.52 ± 0.04 | 48.1 ± 3.8 |
| TM21 | 0.66 ± 0.08 | 0.99 ± 0.04 | 56.8 ± 5.0 |

[a] Ref. [34].

The immiscibility of hydrophobic solvents in aqueous media allows their use in liquid–liquid extraction processes. Specifically, the mixtures studied here have shown efficiency in the removal of chlorophenols, drugs, organic acids and pesticides from polluted water [28,43,44,47,49,50]. Next, we evaluated the extractions of Q, NF, and TC at $T$ = 298.15 from dilute aqueous mixtures with [TM]ESs and calculated the extraction efficiencies (*EE*) as described in Section 2.4. The partition coefficients ($P_{[TM]ESs/w}$) are also obtained. The results are listed in Table S9 and displayed in Fig. 7b. For Q and NF, the efficiency was similar and ranged from 60 to 81 %. For TC, the EE was up to 46 %. For all drugs, it increased with increasing thymol composition. Solvent properties, such as the density, viscosity or polarity, influence this type of process. Fig. 9 shows that a high density and low viscosity and polarity increased the *EE*. The relative solubility had a lower effect.

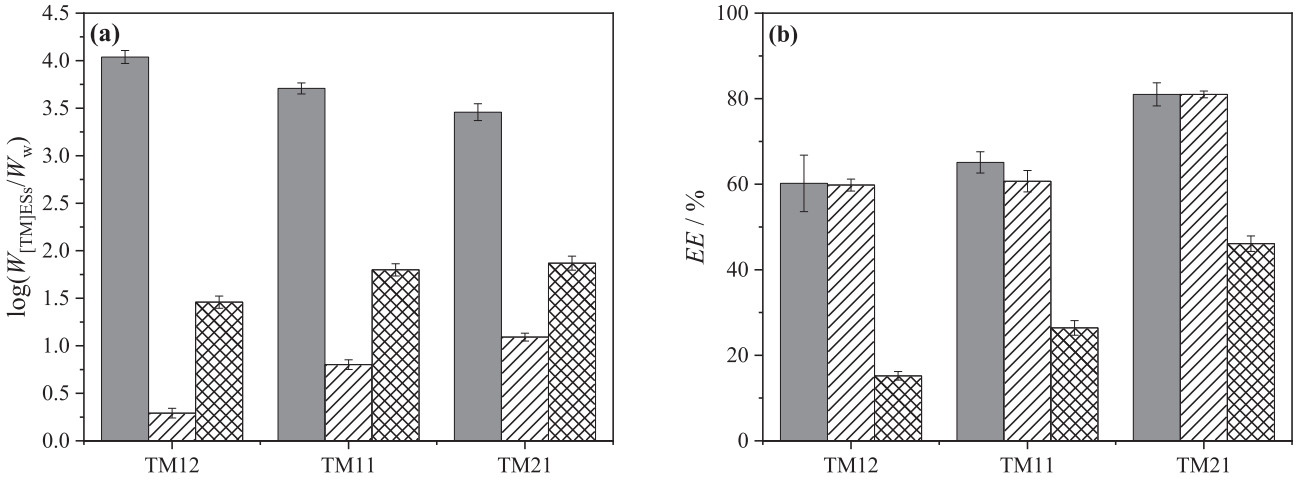


**Fig. 7.** (a) Logarithmic ratio between the solubilities of several drugs in the [TM]ESs, $W_{[TM]ESs}$, and water, $W_w$. (b) Extraction efficiency of [TM]ESs to remove several drugs from water. (▩), Q; (▨), NF; and (▨), TC. $T$ = 298.15$K$ mass ratio 1:1.

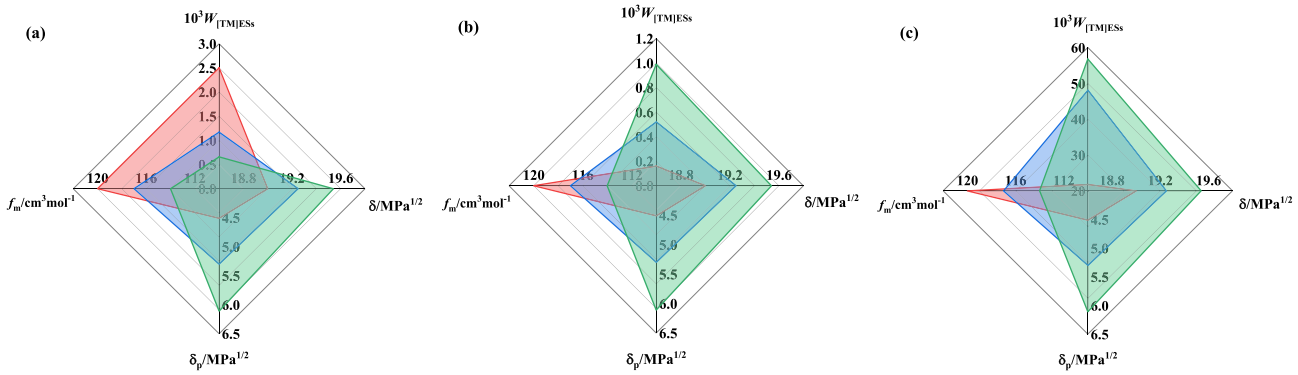


**Fig. 8.** Effects of the free volume, solubility parameter and polar contribution parameter of [TM]ESs on the solubility of drugs. (a), Q; (b), NF; and (c), TC. (▭), TM12; (▭), TM11; (▭), TM21. T= 298.15 K.

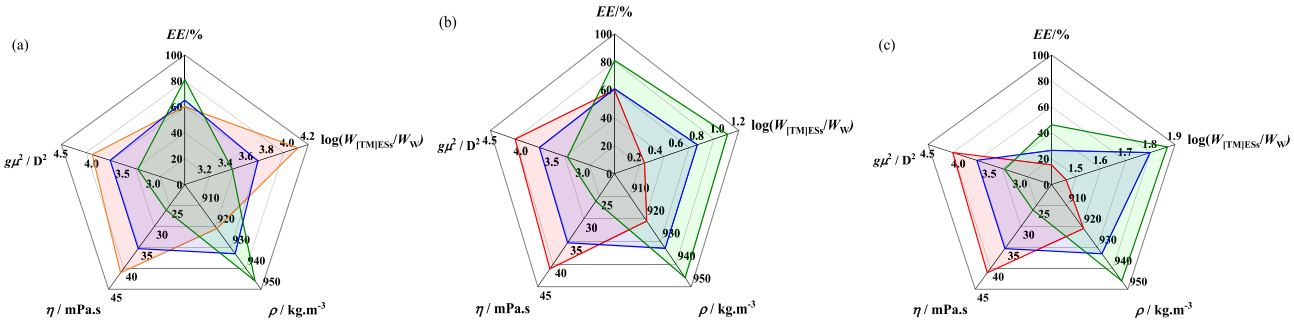


**Fig. 9.** Effects of the [TM]ES properties (solubility ratio, density, viscosity and orientational dipolar parameter) on the drug extraction efficiency. (a), Q; (b), NF; and (c), TC. (▭), TM12; (▭), TM11; (▭), TM21. $T$ = 298.15 K; mass ratio 1:1.

## 4. Conclusions

To achieve the first objective of this work, we studied the thermophysical behaviour of a hydrophobic eutectic system containing thymol and l-menthol ([TM]ESs). The diagram of the solid–liquid phase was measured and compared with the one calculated assuming ideal behaviour. The SLE was correlated with NRTL model and PC-SAFT EoS. For three mixtures of this system with molar ratios of (1:2), (1:1) and (2:1), several properties at 0.1 MPa and over a wide range of temperatures were determined: density, speed of sound, refraction index, isobaric heat capacity, static permittivity, surface tension and viscosity. Additionally, densities up to 65 MPa were measured. Correlations and calculations were performed on the experimental data. Therefore, the internal pressure, intermolecular free length, orientational dipolar parameter, enthalpy and entropy of the surface, critical temperature, and activation energy of the viscous fluid were obtained.

The second aim included an evaluation of the solubilities of the characterized mixtures. The Hildebrand and Hansen solubility parameters were estimated from the experimental above data. The thermodynamic solubilities of quercetin (Q), nitrofurantoin (NF), and tetracycline (TC) in the [TM]ESs were measured and discussed. Finally, their extraction from the aqueous medium was carried out using the hydrophobic character of these liquids.

The SLE showed a strong interaction between both components that prevented the crystallization of the eutectic fraction and caused a negative deviation from the ideal behaviour. Then, the system thymol + menthol can be named a deep eutectic solvent. At any pressure and temperature within the range of this work, the densities were sufficiently lower than those of water to ensure a correct phase separation in liquid–liquid processes. Moreover, the most compact and structured mixture was that with the highest thymol ratio. Conversely, it was the least polar and viscous. Regarding the fluidity, a temperature higher than 288 K would assure an adequate functionality of these mixtures. No appreciable effect of the composition on the solubility parameters was observed. The solubility of Q in [TM]ESs was $10^4$-fold higher than that in water, being favoured in the least compact mixture. For NF and TC, the increase was lower, and the enthalpic effect was more significant. A high density and limited viscosity and polarity increased the extraction efficiencies of these compounds from contaminated water. For Q and NF, the eutectic system showed high efficiencies, up to 81 %, and a medium efficiency was achieved for TC, up to 46 %.

## CRediT authorship contribution statement

**Fernando Bergua:** Investigation, Formal analysis. **Miguel Castro:** Investigation, Methodology. **Carlos Lafuente:** Validation, Writing – original draft, Funding acquisition. **Manuela Artal:** Project administration, Writing – original draft, Writing – review & editing.

## Data availability

Data are in the Supplementary File

## Declaration of Competing Interest

The authors declare that they have no known competing financial interests or personal relationships that could have appeared to influence the work reported in this paper.

## Acknowledgments

PLATON research group acknowledges financial support from Gobierno de Aragón and Fondo Social Europeo "Construyendo Europa desde Aragón" E31_20R.

## Appendix A. Supplementary material

Supplementary data to this article can be found online at https://doi.org/10.1016/j.molliq.2022.120789.

## References

[1] P. Harten, T. Martin, M. Gonzalez, D. Young, The software tool to find greener solvent replacements, PARIS III, Environ. Prog. Sustain Energy 39 (2020) 1–7, https://doi.org/10.1002/ep.13331.
[2] K.H. Kim, T. Dutta, J. Sun, B. Simmons, S. Singh, Biomass pretreatment using deep eutectic solvents from lignin derived phenols, Green Chem. 20 (2018) 809–815, https://doi.org/10.1039/C7GC03029K.
[3] F.P. Byrne, S. Jin, G. Paggiola, T.H.M. Petchey, J.H. Clark, T.J. Farmer, A.J. Hunt, C. Robert McElroy, J. Sherwood, Tools and techniques for solvent selection: green solvent selection guides, Sustain. Chem. Process 4 (1) (2016).
[4] J. Esteban, A.J. Vorholt, W. Leitner, An overview of the biphasic dehydration of sugars to 5-hydroxymethylfurfural and furfural: a rational selection of solvents using COSMO-RS and selection guides, Green Chem. 22 (2020) 2097–2128, https://doi.org/10.1039/C9GC04208C.
[5] A.P. Abbott, E.I. Ahmed, K. Prasad, I.B. Qader, K.S. Ryder, Liquid pharmaceuticals formulation by eutectic formation, Fluid Phase Equilib. 448 (2017) 2–8, https://doi.org/10.1016/j.fluid.2017.05.009.
[6] C.W. Pouton, Formulation of poorly water-soluble drugs for oral administration: Physicochemical and physiological issues and the lipid formulation classification system, Eur. J. Pharm. Sci. 29 (2006) 278–287, https://doi.org/10.1016/j.ejps.2006.04.016.
[7] K. Pathak, Effective formulation strategies for poorly water soluble drugs, in: Adv. Challenges Pharm. Technol., Elsevier, 2021, pp. 181–228, doi: 10.1016/B978-0-12-820043-8.00004-9.
[8] S. Emami, A. Shayanfar, Deep eutectic solvents for pharmaceutical formulation and drug delivery applications, Pharm. Dev. Technol. 25 (2020) 779–796, https://doi.org/10.1080/10837450.2020.1735414.
[9] G. Moradi, M. Rahimi, S. Zinadini, M. Shamsipur, N. Babajani, Natural deep eutectic solvent modified nanofiltration membranes with superior antifouling properties for pharmaceutical wastewater treatment, Chem. Eng. J. 448 (2022) 137704.

[10] T. Moufawad, M. Costa Gomes, S. Fourmentin, Deep eutectic solvents as absorbents for VOC and VOC mixtures in static and dynamic processes, Chem. Eng. J. 448 (2022) 137619.
[11] T.R. Sekharan, R.M. Chandira, S. Tamilvanan, S.C. Rajesh, B.S. Venkateswarlu, Deep eutectic solvents as an alternate to other harmful solvents, Biointerface Res. Appl. Chem. 12 (2022) 847–860, https://doi.org/10.33263/BRIAC121.847860.
[12] S.C. Cunha, J.O. Fernandes, Extraction techniques with deep eutectic solvents, TrAC - Trends Anal. Chem. 105 (2018) 225–239, https://doi.org/10.1016/j.trac.2018.05.001.
[13] R. Abro, N. Kiran, S. Ahmed, A. Muhammad, A.S. Jatoi, S.A. Mazari, U. Salma, N. V. Plechkova, Extractive desulfurization of fuel oils using deep eutectic solvents – a comprehensive review, J. Environ. Chem. Eng. 10 (2022) 107369, https://doi.org/10.1016/j.jece.2022.107369.
[14] A.A.A. Mutalib, N.F. Jaafar, Potential of deep eutectic solvent in photocatalyst fabrication methods for water pollutant degradation: a review, J. Environ. Chem. Eng. 10 (3) (2022) 107422.
[15] M.K. Najaf-Abadi, B. Ghobadian, M. Dehghani-Soufi, A review on application of deep eutectic solvents as green catalysts and co-solvents in biodiesel production and purification processes, Biomass Convers. Biorefinery. (2022), https://doi.org/10.1007/s13399-022-02644-5.
[16] V. Andruch, A. Varfalvyová, R. Halko, N. Jatkowska, J. Płotka-Wasylka, Application of deep eutectic solvents in bioanalysis, TrAC Trends Anal. Chem. 154 (2022) 116660, https://doi.org/10.1016/j.trac.2022.116660.
[17] Y. Liu, J.B. Friesen, J.B. McAlpine, D.C. Lankin, S.N. Chen, G.F. Pauli, Natural deep eutectic solvents: properties, applications, and perspectives, J. Nat. Prod. 81 (2018) 679–690, https://doi.org/10.1021/acs.jnatprod.7b00945.
[18] M.S. Álvarez, Y. Zhang, Sketching neoteric solvents for boosting drugs bioavailability, J. Control. Release. 311–312 (2019) 225–232, https://doi.org/10.1016/j.jconrel.2019.09.008.
[19] N. Mustafa, V. Spelbos, G.-J. Witkamp, R. Verpoorte, Y. Choi, Solubility and stability of some pharmaceuticals in natural deep eutectic solvents-based formulations, Molecules 26 (2021) 2645, https://doi.org/10.3390/molecules26092645.
[20] M.Q. Farooq, N.M. Abbasi, E.A. Smith, J.W. Petrich, J.L. Anderson, Characterizing the solvation characteristics of deep eutectic solvents composed of active pharmaceutical ingredients as a hydrogen bond donor and/or acceptor, ACS Sustain. Chem. Eng. 10 (2022) 3066–3078, https://doi.org/10.1021/acssuschemeng.1c08675.
[21] B. Olivares, F. Martínez, L. Rivas, C. Calderón, J.M. Munita, P.R. Campodonico, A natural deep eutectic solvent formulated to stabilize β-lactam antibiotics, Sci. Rep. 8 (2018) 14900, https://doi.org/10.1038/s41598-018-33148-w.
[22] I.M. Aroso, R. Craveiro, Â. Rocha, M. Dionísio, S. Barreiros, R.L. Reis, A. Paiva, A. R.C. Duarte, Design of controlled release systems for THEDES—therapeutic deep eutectic solvents, using supercritical fluid technology, Int. J. Pharm. 492 (2015) 73–79, https://doi.org/10.1016/j.ijpharm.2015.06.038.
[23] S. Fiala, S.A. Jones, M.B. Brown, A fundamental investigation into the effects of eutectic formation on transmembrane transport, Int. J. Pharm. 393 (2010) 68–73, https://doi.org/10.1016/j.ijpharm.2010.04.001.
[24] A. Brodin, A. Nyqvist-Mayer, T. Wadsten, B. Forslund, F. Broberg, Phase diagram and aqueous solubility of the lidocaine-prilocaine binary system, J. Pharm. Sci. 73 (1984) 481–484, https://doi.org/10.1002/jps.2600730413.
[25] G.M.E. EhrenströmReizRNA, S.L.A. Reiz, EMLA - a eutectic mixture of local anaesthetics for topical anaesthesia, Acta Anaesthesiol. Scand. 26 (1982) 596–598, https://doi.org/10.1111/j.1399-6576.1982.tb01822.x.
[26] D. O'Flynn, J. Lawler, A. Yusuf, A. Parle-McDermott, D. Harold, T. Mc Cloughlin, L. Holland, F. Regan, B. White, A review of pharmaceutical occurrence and pathways in the aquatic environment in the context of a changing climate and the COVID-19 pandemic, Anal. Methods. 13 (2021) 575–594, https://doi.org/10.1039/D0AY02098B.
[27] D.J.G.P. Van Osch, L.F. Zubeir, A. Van Den Bruinhorst, M.A.A. Rocha, M.C. Kroon, Hydrophobic Deep Eutectic Solvents : Water- Immiscible Extractants, (2015) 1–36, doi: 10.1039/C5GC01451D.
[28] D.J.G.P. Van Osch, C.H.J.T. Dietz, J. Van Spronsen, M.C. Kroon, F. Gallucci, M. Van Sint Annaland, R. Tuinier, A search for natural hydrophobic deep eutectic solvents based on natural components, ACS Sustain. Chem. Eng. 7 (2019) 2933–2942, https://doi.org/10.1021/acssuschemeng.8b03520.
[29] M. Marchel, H. Cieśliński, G. Boczkaj, Deep eutectic solvents microbial toxicity: current state of art and critical evaluation of testing methods, J. Hazard. Mater. 425 (2022) 127963.
[30] D. Rodríguez-Llorente, A. Cañada-Barcala, S. Álvarez-Torrellas, V.I. Águeda, J. García, M. Larriba, A review of the use of eutectic solvents, terpenes and terpenoids in liquid–liquid extraction processes, Processes 8 (2020) 1–54, https://doi.org/10.3390/pr8101220.
[31] R. Cañadas, M. González-Miquel, E.J. González, I. Díaz, M. Rodríguez, Overview of neoteric solvents as extractants in food industry: a focus on phenolic compounds separation from liquid streams, Food Res. Int. 136 (2020) 109558, https://doi.org/10.1016/j.foodres.2020.109558.
[32] P. Makoś, E. Słupek, J. Gębicki, Hydrophobic deep eutectic solvents in microextraction techniques–a review, Microchem. J. 152 (2020) 104384, https://doi.org/10.1016/j.microc.2019.104384.
[33] J. Lee, D. Jung, K. Park, Hydrophobic deep eutectic solvents for the extraction of organic and inorganic analytes from aqueous environments, TrAC - Trends Anal. Chem. 118 (2019) 853–868, https://doi.org/10.1016/j.trac.2019.07.008.
[34] F. Bergua, M. Castro, J. Muñoz-Embid, C. Lafuente, M. Artal, Hydrophobic eutectic solvents: thermophysical study and application in removal of pharmaceutical products from water, Chem. Eng. J. 411 (2021) 128472, https://doi.org/10.1016/j.cej.2021.128472.
[35] F. Bergua, M. Castro, J. Muñoz-Embid, C. Lafuente, M. Artal, L-menthol-based eutectic solvents: characterization and application in the removal of drugs from water, J. Mol. Liq. 352 (2022) 118754, https://doi.org/10.1016/j.molliq.2022.118754.
[36] M. Zielińska-Błajet, P. Pietrusiak, J. Feder-Kubis, Selected monocyclic monoterpenes and their derivatives as effective anticancer therapeutic agents, Int. J. Mol. Sci. 22 (2021) 4763, https://doi.org/10.3390/ijms22094763.
[37] U.T. Syed, I.C. Leonardo, G. Mendoza, F.B. Gaspar, E. Gámez, R.M. Huertas, M.T. B. Crespo, M. Arruebo, J.G. Crespo, V. Sebastian, C. Brazinha, On the role of components of therapeutic hydrophobic deep eutectic solvent-based nanoemulsions sustainably produced by membrane-assisted nanoemulsification for enhanced antimicrobial activity, Sep. Purif. Technol. 285 (2022) 120319, https://doi.org/10.1016/j.seppur.2021.120319.
[38] D.O. Abranches, M.A.R. Martins, L.P. Silva, N. Schaeffer, S.P. Pinho, J.A.P. Coutinho, Phenolic hydrogen bond donors in the formation of non-ionic deep eutectic solvents: the quest for type v des, Chem. Commun. 55 (2019) 10253–10256, https://doi.org/10.1039/c9cc04846d.
[39] A. Alhadid, L. Mokrushina, M. Minceva, Formation of glassy phases and polymorphism in deep eutectic solvents, J. Mol. Liq. 314 (2020) 113667.
[40] A. Alhadid, C. Jandl, L. Mokrushina, M. Minceva, Experimental investigation and modeling of cocrystal formation in L-menthol/thymol eutectic system, Cryst. Growth Des. 21 (2021) 6083–6091, https://doi.org/10.1021/acs.cgd.1c00306.
[41] N. Schaeffer, D.O. Abranches, L.P. Silva, M.A.R. Martins, P.J. Carvalho, O. Russina, A. Triolo, L. Paccou, Y. Guinet, A. Hedoux, J.A.P. Coutinho, Non-ideality in thymol + menthol type v deep eutectic solvents, ACS Sustain. Chem. Eng. 9 (2021) 2203–2211, https://doi.org/10.1021/acssuschemeng.0c07874.
[42] M.A.R. Martins, L.P. Silva, N. Schaeffer, D.O. Abranches, G.J. Maximo, S.P. Pinho, J.A.P. Coutinho, Greener terpene-terpene eutectic mixtures as hydrophobic solvents, ACS Sustain. Chem. Eng. 7 (2019) 17414–17423, https://doi.org/10.1021/acssuschemeng.9b04614.
[43] I. Adeyemi, R. Sulaiman, M. Almazroui, A. Al-Hammadi, I.M. AlNashef, Removal of chlorophenols from aqueous media with hydrophobic deep eutectic solvents: experimental study and COSMO RS evaluation, J. Mol. Liq. 311 (2020) 113180, https://doi.org/10.1016/j.molliq.2020.113180.
[44] S.A. Mat Hussin, P. Varanusupakul, S. Shahabuddin, B. Yih Hui, S. Mohamad, Synthesis and characterization of green menthol-based low transition temperature mixture with tunable thermophysical properties as hydrophobic low viscosity solvent, J. Mol. Liq. 308 (2020) 113015, https://doi.org/10.1016/j.molliq.2020.113015.
[45] K. Xin, I. Roghair, F. Gallucci, M. van Sint Annaland, Total vapor pressure of hydrophobic deep eutectic solvents: experiments and modelling, J. Mol. Liq. 325 (2021) 115227, https://doi.org/10.1016/j.molliq.2020.115227.
[46] T. Raja Sekharan, R. Margret Chandira, S.C. Rajesh, S. Tamilvanan, C.T. Vijayakumar, B.S. Venkateswarlu, Ph, viscosity of hydrophobic based natural deep eutectic solvents and the effect of curcumin solubility in it, Biointerface Res. Appl. Chem. 11 (2021) 14620–14633, https://doi.org/10.33263/BRIAC116.1462014633.
[47] K.e. Li, Y. Jin, D. Jung, K. Park, H. Kim, J. Lee, In situ formation of thymol-based hydrophobic deep eutectic solvents: application to antibiotics analysis in surface water based on liquid-liquid microextraction followed by liquid chromatography, J. Chromatogr. A. 1614 (2020) 460730.
[48] T. Brouwer, B.C. Dielis, J.M. Bock, B. Schuur, Hydrophobic deep eutectic solvents for the recovery of bio-based chemicals: solid–liquid equilibria and liquid–liquid extraction, Processes 9 (5) (2021) 796.
[49] F.A. Hansen, E. Santigosa-Murillo, M. Ramos-Payán, M. Muñoz, E. Leere Øiestad, S. Pedersen-Bjergaard, Electromembrane extraction using deep eutectic solvents as the liquid membrane, Anal. Chim. Acta. 1143 (2021) 109–116, https://doi.org/10.1016/j.aca.2020.11.044.
[50] Á. Santana-Mayor, B. Socas-Rodríguez, R. Rodríguez-Ramos, A.V. Herrera-Herrera, M.Á. Rodríguez-Delgado, Quality assessment of environmental water by a simple and fast non-ionic hydrophobic natural deep eutectic solvent-based extraction procedure combined with liquid chromatography tandem mass spectrometry for the determination of plastic migrants, Anal. Bioanal. Chem. 413 (2021) 1967–1981, https://doi.org/10.1007/s00216-021-03166-1.
[51] U.L. Abbas, Q. Qiao, M.T. Nguyen, J. Shi, Q. Shao, Molecular dynamics simulations of heterogeneous hydrogen bond environment in hydrophobic deep eutectic solvents, AIChE J. 68 (2022), https://doi.org/10.1002/aic.17382.
[52] N.H.C.S. Silva, E.S. Morais, C.S.R. Freire, M.G. Freire, A.J.D. Silvestre, Extraction of high value triterpenic acids from Eucalyptus globulus biomass using hydrophobic deep eutectic solvents, Molecules 25 (1) (2020) 210.
[53] C.G. Le Fèvre, R.J.W. Le Fèvre, K.W. Robertson, 107. The dipole moments of p-cymene; 2- and 3-halogeno-p-cymenes, carvacrol, and thymol; p-ethyltoluene; p-tert.-butyltoluene, 1: 3-dimethyl-5-tert.- butylbenzene, tert.-butylbenzene and its p-nitro-derivative, J. Chem. Soc. (1935) 480–488, https://doi.org/10.1039/JR9350000480.
[54] R. Maruchenko, P. Espeau, Revised phase diagrams based on racemic ibuprofen with thymol and l-menthol, J. Therm. Anal. Calorim. 145 (6) (2021) 3087–3091.
[55] Stenutz, n.d. Available from: <http://www.stenutz.eu/chem/>.
[56] Pubchem, n.d. Available from: <https://pubchem.ncbi.nlm.nih.gov/>.
[57] A.M. Mendoza-Wilson, D. Glossman-Mitnik, CHIH-DFT study of the electronic properties and chemical reactivity of quercetin, J. Mol. Struct. THEOCHEM. 716 (2005) 67–72, https://doi.org/10.1016/j.theochem.2004.10.083.

[58] U. of A. A.M. Matuszek, Defining Known Drug Space by DFT based molecular descriptors. Virtual screening for novel Atg5-Atg16 complex inhibitors for autophagy modulation, 2014.
[59] L. Percevault, A. Jani, T. Sohier, L. Noirez, L. Paquin, F. Gauffre, D. Morineau, Do deep eutectic solvents form uniform mixtures beyond molecular microheterogeneities?, J Phys. Chem. B. 124 (2020) 9126–9135, https://doi.org/10.1021/acs.jpcb.0c06317.
[60] H. Renon, J.M. Prausnitz, Local compositions in thermodynamic excess functions for liquid mixtures, AIChE J. 14 (1968) 135–144, https://doi.org/10.1002/aic.690140124.
[61] J. Gross, G. Sadowski, Perturbed-chain SAFT: An equation of state based on a perturbation theory for chain molecules, Ind. Eng. Chem. Res. 40 (2001) 1244–1260, https://doi.org/10.1021/ie0003887.
[62] J. Gross, G. Sadowski, Application of the perturbed-chain SAFT equation of state to associating systems, Ind. Eng. Chem. Res. 41 (2002) 5510–5515, https://doi.org/10.1021/ie010954d.
[63] B. Jacobson, Ultrasonic Velocity in Liquids and Liquid Mixtures, J. Chem. Phys. 20 (1952) 927–928, https://doi.org/10.1063/1.1700615.
[64] H. Fröhlich, General theory of the static dielectric constant, Trans. Faraday Soc. 44 (1948) 238–243, https://doi.org/10.1039/TF9484400238.
[65] R. Bouteloup, D. Mathieu, Predicting dielectric constants of pure liquids: Fragment-based Kirkwood-Fröhlich model applicable over a wide range of polarity, Phys. Chem. Chem. Phys. 21 (2019) 11043–11057, https://doi.org/10.1039/c9cp01704f.
[66] M. Taherzadeh, R. Haghbakhsh, A.R.C. Duarte, S. Raeissi, Estimation of the heat capacities of deep eutectic solvents, J. Mol. Liq. 307 (2020) 112940, https://doi.org/10.1016/j.molliq.2020.112940.
[67] E.A.A. Guggenheim, The principle of corresponding states, J. Chem. Phys. 13 (1945) 253–261, https://doi.org/10.1063/1.1724033.
[68] J.L.L. Shereshefsky, Surface tension of saturated vapors and the equation of Eötvos, J. Phys. Chem. 35 (1930) 1712–1720, https://doi.org/10.1021/j150324a014.
[69] A.H. Pelofsky, Surface Tension-Viscosity Relation for Liquids, J. Chem. Eng. Data. 11 (1966) 394–397, https://doi.org/10.1021/je60030a031.
[70] J.H. Hildebrand, Solubility of non-electrolytes. By J. H. Hildebrand, Ph.D. 2nd ed. Pp. 203. New York: Reinhold Publishing Corp., London: Chapman & Hall, Ltd., 1936. 22s. 6d, J. Soc. Chem. Ind. 55 (1936) 665–665, doi: 10.1002/jctb.5000553408.
[71] C.N. Pereira, G.C. Vebber, An innovative model for correlating surface tension, solubility parameters, molar volume and ratio of the coordination numbers of liquid metals, based on Stefan's rule, Surf. Interfaces 13 (2018) 51–57, https://doi.org/10.1016/j.surfin.2018.07.004.
[72] C.M. Hansen, The three dimensional solubility parameter and solvent diffusion coefficient. Their importance in surface coating formulation, J. Paint Technol. (1967) 104.
[73] C.D. Vaughan, Using solubility parameters in cosmetics formulation, J. Soc. Cosmet. Chem. Japan. 36 (1985) 319–333.
[74] C.H. Hansen, C.M.; Beerbower, Solubility parameters, Kirk-Othmer Encycl. Chem. Technol., New York, 1971.
[75] Hansen, K. Skaarup, The three dimensional solubility parameter-key to paint component affinities: III; Independent calculation of the parameter components, J. Paint Technol. 37 (1967) 511–515.
[76] D. Mathieu, Pencil and paper estimation of Hansen solubility parameters, ACS Omega 3 (2018) 17049–17056, https://doi.org/10.1021/acsomega.8b02601.